Proceedings of the 2003 IEEE
International Conference on Robotics & Automation
Taipei, Taiwan, September 14-19, 2003

Probabilistic Models of Dead-Reckoning Error in Nonholonomic Mobile Robots

Yu Zhou
Department of Mechanical Engineering
The Johns Hopkins University
Baltimore, MD 21218
USA
yuzhou@titan.me.jhu.edu

Gregory S. Chirikjian
Department of Mechanical Engineering
The Johns Hopkins University
Baltimore, MD 21218
USA
gregc@jhu.edu

Abstract **— In this paper, dead-reckoning error in mobile robots is studied in the context of several different models. These models are derived first in the form of stochastic differential equations (SDEs). Corresponding Fokker-Planck equations are derived, and desired probability density functions (PDFs) of robot pose are computed by using the Fourier transform for SE(2).**

I. INTRODUCTION

Many mobile robot tasks require that the robot have some knowledge of its position. Because of its simplicity, dead-reckoning is widely used to provide such information. The position of a mobile robot in a global reference frame is determined by summing the incremental movements, e.g. counting the revolutions of the robot wheels. Since sensors are not perfect, errors accumulate in dead-reckoning pose estimation.

Efforts are often made to reduce dead-reckoning error. Many systems use readings from extra sensors, such as ultrasonic sensors [1] and fiber-optic gyroscopes [2], together with dead-reckoning data to update robot location. This is often implemented by utilizing Kalman filtering. Vision-based techniques are also used to assist the dead-reckoning process [3,4]. With neural networks detecting the wheel slip and estimating the linear velocity of the wheels, the performance of conventional dead-reckoning estimation is improved [5]. For a class of dual-drive compliant linkage robots, an internal position error correction method was proposed, based on the measurement of the difference in motion between the two connected carts [6]. Dead-reckoning is also applied to robot map generation. Based on the observed analogy between graphs modeling the environment and truss structures, the method of elastic correction was proposed to correct dead-reckoning errors made during exploration with a robot capable of identifying landmarks [7]. On the side of probabilistic methods, a map with spatial occupancy representation, which defines the probability of occupancy of each cell in space, can be estimated by doing Markov model-based searches of the next optimal robot position [8-10].

Since many mobile robots operate under noisy situations, a probability error model was developed to give an estimate of robot location with uncertainty [11], which is modeled as a set of equal-error-probability ellipse isolines. In practice, the probability of robot pose can be more complex, depending on different probabilistic models. This paper examines three models, the kinematic disk, cart and car, and develops an algorithm to obtain the probability distribution of robot position and orientation caused by noise in the direct reading of wheel speeds.

II. STOCHASTIC DIFFERENTIAL EQUATIONS

To generate the probability density function of pose for a nonholonomic system subjected to white noise, a system of SDEs needs to be constructed. Any system of SDEs can be written in the standard form [12]

$$d\mathbf{x} = \mathbf{a}(\mathbf{x}, t)dt + \mathbf{B}(\mathbf{x}, t)d\mathbf{w}(t), \quad (1)$$

where in the case of a mobile robot $\mathbf{x}=(x,y,\theta)^{\mathrm{T}}$ denotes the pose of the robot moving in a plane, $d\mathbf{w}$ is a vector consisting of uncorrelated normalized white noises, **a** is called the drift vector, and **B** is called the diffusion matrix. Equation (1) reflects the fact that for a mobile robot subjected to stochastic forcing, the evolution of the pose density is really a diffusion process.

In this section, the SDEs for the kinematic disk, cart and car moving in the plane are derived respectively.

A. SDE of a Rolling Disk

As a widely studied classical and simple model, the nonholonomic constraint for a rolling disk with deterministic spinning arises by allowing it to roll but not slip (Fig.1)

$$dx = r\,\omega(t)\cos\theta dt, \quad (2)$$

$$dy = r\,\omega(t)\sin\theta dt, \quad (3)$$

where θ is the heading angle of the disk plane with respect to its initial orientation, $\omega(t)=d\phi/dt$ denotes the rate of spinning of the disk about its axle, and r the radius of the disk.

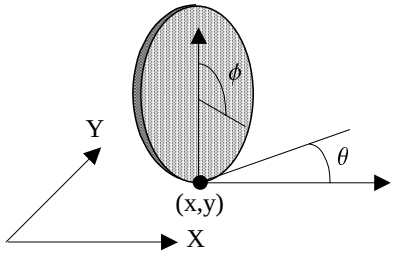

Fig.1 Kinematic disk moving on a plane

Assuming that the orientation of the rolling disk is governed by a Wiener process

$$d\theta = \sqrt{D}dw, \tag{4}$$

one obtains a system of SDEs for the rolling disk with deterministic spinning and random heading [13]

$$\begin{pmatrix} dx \\ dy \\ d\theta \end{pmatrix} = \begin{pmatrix} r\omega(t)\cos\theta \\ r\omega(t)\sin\theta \\ 0 \end{pmatrix} dt + \sqrt{D}\begin{pmatrix} 0 \\ 0 \\ 1 \end{pmatrix} dw. \tag{5}$$

B. SDE of a Kinematic Cart

As another model of the mobile robots under discussion, the kinematic cart (Fig.2) has two wheels which can roll at different speeds, and therefore change the orientation of the cart from time to time. The nonholonomic constraint for the cart arises by allowing the wheels to roll but not slip. Moreover, connected by an axle, the wheels steer together. As a result, the sideway velocity of the cart is zero, and the cart can only move in the direction of the body orientation.

For each wheel, (2) and (3) can be rewritten as

$$dx_i = r\cos\theta\, d\phi_i, \tag{6}$$

$$dy_i = r\sin\theta\, d\phi_i, \tag{7}$$

where i=1 or 2. For the whole system, one obtains

$$dx = \frac{dx_1 + dx_2}{2}, \tag{8}$$

$$dy = \frac{dy_1 + dy_2}{2}, \tag{9}$$

$$ld\theta = rd\phi_1 - rd\phi_2, \tag{10}$$

where (x,y) denotes the position of the midpoint of the axle, and l is the length of the axle. Therefore, one obtains

$$dx = \frac{r\cos\theta(d\phi_1 + d\phi_2)}{2}, \tag{11}$$

$$dy = \frac{r\sin\theta(d\phi_1 + d\phi_2)}{2}, \tag{12}$$

$$d\theta = \frac{r(d\phi_1 - d\phi_2)}{l}. \tag{13}$$

Assuming the rolling speeds of the wheels are governed by a deterministic and stochastic part

$$d\phi_1 = \omega(t)dt + \sqrt{D}dw_1, \tag{14}$$

$$d\phi_2 = \omega(t)dt + \sqrt{D}dw_2, \tag{15}$$

where $\omega(t)$ denotes the deterministic part of the rolling speed, and dw_i are Wiener processes, one obtains the SDEs of the kinematic cart

$$\begin{pmatrix} dx \\ dy \\ d\theta \end{pmatrix} = \begin{pmatrix} r\omega(t)\cos\theta \\ r\omega(t)\sin\theta \\ 0 \end{pmatrix} dt + \sqrt{D}\begin{pmatrix} \frac{r}{2}\cos\theta & \frac{r}{2}\cos\theta \\ \frac{r}{2}\sin\theta & \frac{r}{2}\sin\theta \\ \frac{r}{l} & -\frac{r}{l} \end{pmatrix} \begin{pmatrix} dw_1 \\ dw_2 \end{pmatrix}. \tag{16}$$

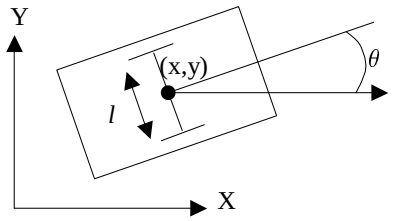

Fig.2 Kinematic cart moving on a plane

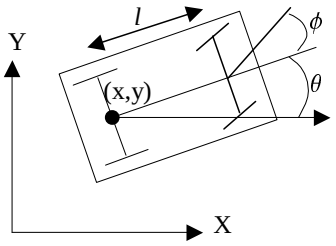

Fig.3 Kinematic car moving on a plane

C. SDE of a Kinematic Car

Another model of mobile robots is the kinematic car (Fig.3). It has two rear wheels which roll together, and two front wheels which steer together. The nonholonomic constraint for the car arises by replacing each of these two sets of wheels with a single imaginary wheel centered along their axles and allowing the wheels to roll but not slip, i.e. [14]

$$dx\sin\theta - dy\cos\theta = 0, \tag{17}$$

$$dx\sin(\theta+\phi) - dy\cos(\theta+\phi) - ld\theta\cos\phi = 0. \tag{18}$$

Here (x,y) is the position of the midpoint of the rear axle, θ is the angle of the car body with respect to its initial orientation, and ϕ is the steering angle with respect to the car body. Here,

$$dx = r\omega(t)\cos\theta dt, \tag{19}$$

$$dy = r\omega(t)\sin\theta dt, \tag{20}$$

where $\omega(t)$ denotes the rolling speed of the rear wheels.

Assuming that the steering of the car is governed by a deterministic part and a Wiener process

$$d\phi = \xi(t)dt + \sqrt{D}dw, \tag{21}$$

one obtains a system of SDEs for the car

$$\begin{pmatrix} dx \\ dy \\ d\theta \\ d\phi \end{pmatrix} = \begin{pmatrix} r\omega(t)\cos\theta \\ r\omega(t)\sin\theta \\ \frac{r}{l}\omega(t)\tan\phi \\ \xi(t) \end{pmatrix} dt + \sqrt{D}\begin{pmatrix} 0 \\ 0 \\ 0 \\ 1 \end{pmatrix} dw. \tag{22}$$

III. FOKKER-PLANCK EQUATIONS

To calculate the PDFs as a continuous function of robot pose and time, the Fokker-Planck equations corresponding to the SDEs of different models need to be solved. The solution of a Fokker-Planck equation is a time evolving PDF of robot

pose. Applying Ito's method to (1), the corresponding Fokker-Planck equation is [12]

$$\frac{\partial f}{\partial t} = -\sum_i \frac{\partial}{\partial x_i}(a_i(\mathbf{x},t) f) + \frac{1}{2}\sum_i \sum_j \frac{\partial^2}{\partial x_i \partial x_j}((\mathbf{B}(\mathbf{x},t)\mathbf{B}^T(\mathbf{x},t))_{ij} f) \quad (23)$$

Applying Stratonovich's method to (1), the corresponding Fokker-Planck equation is [12]

$$\frac{\partial f}{\partial t} = -\sum_i \frac{\partial}{\partial x_i}(a_i(\mathbf{x},t) f) + \frac{1}{2}\sum_i \sum_j \sum_k \frac{\partial}{\partial x_i}(B_{ik} \frac{\partial}{\partial x_j}(B_{jk} f)) \quad (24)$$

From (5), one obtains the same Fokker-Planck equation for the rolling disk with deterministic spinning and random heading using both the Ito and Stratonovich methods

$$\frac{\partial f}{\partial t} = -r\omega(t)\cos\theta \frac{\partial f}{\partial x} - r\omega(t)\sin\theta \frac{\partial f}{\partial y} + \frac{D}{2}\frac{\partial^2 f}{\partial \theta^2}, \quad (25)$$

where $f=f(g(x,y,\theta),t)$ is the desired time-evolving PDF, and $g(x,y,\theta)$ denotes a member of the group of planar rigid-body motion SE(2).

From (11), one obtains the same Fokker-Planck equation for the kinematic cart using both the Ito and Stratonovich methods

$$\frac{\partial f}{\partial t} = -r\omega(t)\cos\theta \frac{\partial f}{\partial x} - r\omega(t)\sin\theta \frac{\partial f}{\partial y} + \frac{D}{2}(\frac{r^2}{2}\cos^2\theta \frac{\partial^2 f}{\partial x^2} + \frac{r^2}{2}\sin 2\theta \frac{\partial^2 f}{\partial x \partial y} + \frac{r^2}{2}\sin^2\theta \frac{\partial^2 f}{\partial y^2} + \frac{2r^2}{l^2}\frac{\partial^2 f}{\partial \theta^2}) \quad (26)$$

From (22), one obtains the same Fokker-Planck equation for the kinematic car using both the Ito and Stratonovich methods

$$\frac{\partial f}{\partial t} = -r\omega(t)\cos\theta \frac{\partial f}{\partial x} - r\omega(t)\sin\theta \frac{\partial f}{\partial y} - \frac{r}{l}\omega(t)\tan\phi \frac{\partial f}{\partial \theta} - \xi(t)\frac{\partial f}{\partial \phi} + \frac{D}{2}\frac{\partial^2 f}{\partial \phi^2} \quad (27)$$

With constant $\omega(t)=v$ and $\xi(t)=0$ (in the case of the car moving in a straight line), (25)- (27) change into the simpler versions:

$$\frac{\partial f}{\partial t} = -rv\cos\theta \frac{\partial f}{\partial x} - rv\sin\theta \frac{\partial f}{\partial y} + \frac{D}{2}\frac{\partial^2 f}{\partial \theta^2}, \quad (28)$$

$$\frac{\partial f}{\partial t} = -rv\cos\theta \frac{\partial f}{\partial x} - rv\sin\theta \frac{\partial f}{\partial y} + \frac{D}{2}(\frac{r^2}{2}\cos^2\theta \frac{\partial^2 f}{\partial x^2} + \frac{r^2}{2}\sin 2\theta \frac{\partial^2 f}{\partial x \partial y} + \frac{r^2}{2}\sin^2\theta \frac{\partial^2 f}{\partial y^2} + \frac{2r^2}{l^2}\frac{\partial^2 f}{\partial \theta^2}), \quad (29)$$

$$\frac{\partial f}{\partial t} = -rv\cos\theta \frac{\partial f}{\partial x} - rv\sin\theta \frac{\partial f}{\partial y} - \frac{rv}{l}\tan\phi \frac{\partial f}{\partial \theta} + \frac{D}{2}\frac{\partial^2 f}{\partial \phi^2}. \quad (30)$$

IV. SOLVING FOKKER-PLANCK EQUATIONS

Since the mobile robots under discussion are modeled by kinematic disks, carts and cars moving in a plane, operational properties of the Fourier transform of functions on SE(2) can be used to solve the Fokker-Planck equations (28)-(30).

A. Operational Properties Used in Solving Fokker-Planck Equations

SE(2) is the group of rigid-body motions in the plane [14,15]. The right differential operators for SE(2) in Cartesian coordinates are [15,16,17]

$$\tilde{X}_1^R = \cos\theta \frac{\partial}{\partial x} + \sin\theta \frac{\partial}{\partial y}, \quad (31)$$

$$\tilde{X}_2^R = -\sin\theta \frac{\partial}{\partial x} + \cos\theta \frac{\partial}{\partial y}, \quad (32)$$

$$\tilde{X}_3^R = \frac{\partial}{\partial \theta}. \quad (33)$$

The Fourier transform on SE(2) is defined as [15]

$$F(f) = \hat{\mathbf{f}}(p) = \int_{SE(2)} f(g)\mathbf{U}(g^{-1}, p)d(g), \quad (34)$$

and its inverse transform is defined as [15]

$$F^{-1}(\hat{\mathbf{f}}) = f(g) = \int_0^\infty trace(\hat{\mathbf{f}}(p)\mathbf{U}(g,p))pdp, \quad (35)$$

where g denotes a member of SE(2), p is the "frequency" introduced by the Fourier transform, and $\mathbf{U}(g,p)$ is an irreducible unitary representation matrix of SE(2). Here the elements of matrix $\mathbf{U}(g,p)$ are given as [15]

$$u_{mn}(g(r,\phi,\theta), p) = i^{(n-m)}e^{-i(n\theta+(m-n)\phi)}J_{n-m}(pr), \quad (36)$$

where $-\infty<m,n<\infty$.

An important operational property of the Fourier transform for SE(2) is [15,16,17]

$$F(\tilde{X}_i^R f) = \boldsymbol{\eta}_i(p)\hat{\mathbf{f}}(p), \quad (37)$$

where $\boldsymbol{\eta}_i(p)$'s are coefficient matrices with elements [16,17]

$$\eta_{1mn}(p) = \frac{p}{2}(\delta_{m,n+1} - \delta_{m,n-1}), \quad (38)$$

$$\eta_{2mn}(p) = \frac{ip}{2}(\delta_{m,n+1} + \delta_{m,n-1}), \quad (39)$$

$$\eta_{3mn}(p) = -im\delta_{m,n}, \quad (40)$$

where δ is the Kronecker delta function.

B. Solving for the Disk Model

By using (31)-(33), one rewrites (28) as

$$\frac{\partial f(g,t)}{\partial t} = (-rv\tilde{X}_1^R + \frac{D}{2}\tilde{X}_3^{R^2})f(g,t). \quad (41)$$

By applying the SE(2) Fourier transform on both sides of (41), one obtains

$$\frac{\partial \hat{\mathbf{f}}(p,t)}{\partial t} = (-rv\boldsymbol{\eta}_1(p) + \frac{D}{2}\boldsymbol{\eta}_3(p)^2)\hat{\mathbf{f}}(p,t). \quad (42)$$

The solution to (42) is

$$\hat{\mathbf{f}}(p,t) = e^{\mathbf{A}(p)t}\hat{\mathbf{f}}(p,0), \tag{43}$$

where

$$\mathbf{A}(p) = -rv\boldsymbol{\eta}_1(p) + \frac{D}{2}\boldsymbol{\eta}_3(p)^2, \tag{44}$$

By setting $x=y=\theta=0$ when $t=0$, the initial condition for (28) is defined as

$$f(g(x,y,\theta);t=0) = \delta(x)\delta(y)\delta(\theta), \tag{45}$$

where δ is the Dirac delta function. As a result, $\hat{\mathbf{f}}(p,0)$ is the identity matrix, and (43) is reduced to

$$\hat{\mathbf{f}}(p,t) = e^{\mathbf{A}(p)t}. \tag{46}$$

By applying the inverse Fourier transform for SE(2) to (46), one obtains the solution to (28)

$$\begin{aligned} & f(g(x,y,\theta),t) \\ &= \int_0^\infty trace(\hat{\mathbf{f}}(p,t)\mathbf{U}(g(x,y,\theta),p)pdp \\ &= \sum_{m\in Z}\sum_{n\in Z}\int_0^\infty \hat{\mathbf{f}}(p,t)_{mn}u_{nm}(g(x,y,\theta),p)pdp \end{aligned}, \tag{47}$$

where Z denotes the set of all integers.

To compute the reduced PDF $f(x,y,t)$, one integrates $f(g(x,y,\theta),t)$ analytically as

$$f(x,y,t) = \int_{-\pi}^{\pi} f(g(x,y,\theta),t)d\theta. \tag{48}$$

Since the matrices $\boldsymbol{\eta}$ and $\mathbf{U}$ are infinite dimensional, we must truncate them to finite dimension as (2L+1) by (2L+1) matrices when doing numerical computations, where L is a chosen integer.

By solving the Fokker-Planck equation (28), one obtains PDFs like those in Fig.3.

C. Solving for the Cart Model

By using (31)-(33), one rewrites (29) as

$$\frac{\partial f(g,t)}{\partial t} = (-rv\tilde{X}_1^R + \frac{D}{2}(\frac{r^2}{2}\tilde{X}_1^{R^2} + \frac{2r^2}{l^2}\tilde{X}_3^{R^2}))f(g,t). \tag{49}$$

By applying the SE(2) Fourier transform on both sides of equation (49), one obtains

$$\frac{\partial \hat{\mathbf{f}}(p,t)}{\partial t} = (-rv\boldsymbol{\eta}_1(p) + \frac{D}{2}(\frac{r^2}{2}\boldsymbol{\eta}_1(p)^2 + \frac{2r^2}{l^2}\boldsymbol{\eta}_3(p)^2))\hat{\mathbf{f}}(p,t). \tag{50}$$

By following the steps in the last subsection, one can obtain the desired PDFs like those in Fig.4.

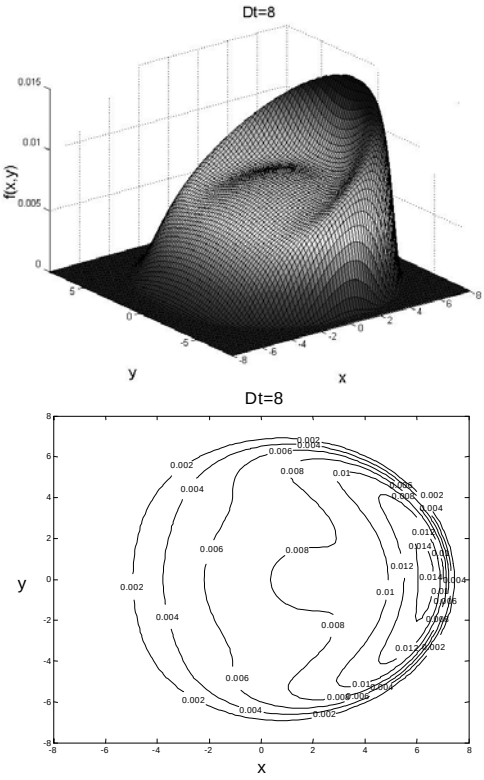

Fig.3 PDF of the position of the disk model when Dt=8 and r=v=1 (L=5)

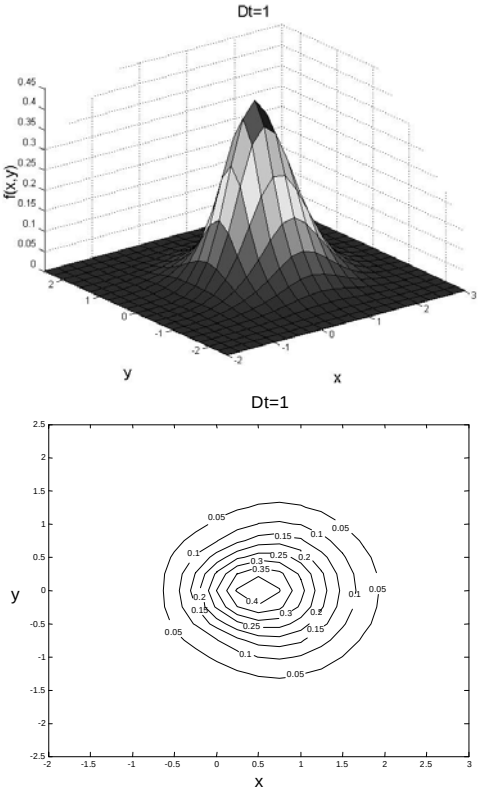

Fig.4 PDF of the position of the cart model when Dt=1 and r=*l*=v=1 (L=3)

D. Solving for the Car Model

By using (31)-(33), one rewrites (30) as

$$\frac{\partial f(g,t)}{\partial t} = (-rvX_1^R - \frac{rv}{l}\tan\phi X_3^R + \frac{D}{2}\frac{\partial^2}{\partial\phi^2}) f(g,t) \cdot \quad (51)$$

Multiplying both sides of (51) by $\cos^2\phi$, one obtains

$$\cos^2\phi\frac{\partial f(g,t)}{\partial t} = (-rv\cos^2\phi X_1^R - \frac{rv}{l}\sin\phi\cos\phi X_3^R + \frac{D}{2}\cos^2\phi\frac{\partial^2}{\partial\phi^2}) f(g,t) \quad (52)$$

By expanding f, $\cos\phi$ and $\sin\phi$ in a Fourier series in ϕ, i.e.

$$f(g) = \sum_{n=-\infty}^{\infty} f_n(g)e^{in\phi}, \quad (53)$$

$$\cos\phi = \frac{e^{i\phi}+e^{-i\phi}}{2}, \quad (54)$$

$$\sin\phi = \frac{e^{i\phi}-e^{-i\phi}}{2}, \quad (55)$$

one obtains

$$\begin{aligned}&\sum_{n=-\infty}^{\infty}(\frac{\partial f_{n-2}(g,t)}{\partial t} + 2\frac{\partial f_n(g,t)}{\partial t} + \frac{\partial f_{n+2}(g,t)}{\partial t})e^{in\phi}\\ &= \sum_{n=-\infty}^{\infty}((-rv\tilde{X}_1^R + i\frac{rv}{l}\tilde{X}_3^R - \frac{D(n-2)^2}{2}) f_{n-2}(g,t)\\ &+ (-2rv\tilde{X}_1^R - Dn^2) f_n(g,t)\\ &+ (-rv\tilde{X}_1^R - i\frac{rv}{l}\tilde{X}_3^R - \frac{D(n+2)^2}{2}) f_{n+2}(g,t))e^{in\phi}\end{aligned}, \quad (56)$$

from which one obtains a system of partial differential equations

$$\begin{aligned}&\frac{\partial f_{n-2}(g,t)}{\partial t} + 2\frac{\partial f_n(g,t)}{\partial t} + \frac{\partial f_{n+2}(g,t)}{\partial t}\\ &= (-rv\tilde{X}_1^R + i\frac{rv}{l}\tilde{X}_3^R - \frac{D(n-2)^2}{2}) f_{n-2}(g,t)\\ &+ (-2rv\tilde{X}_1^R - Dn^2) f_n(g,t)\\ &+ (-rv\tilde{X}_1^R - i\frac{rv}{l}\tilde{X}_3^R - \frac{D(n+2)^2}{2}) f_{n+2}(g,t)\end{aligned}. \quad (57)$$

By applying the SE(2) Fourier transform on both sides of (57), one obtains a new system of differential equations

$$\begin{aligned}&\frac{\partial \hat{\mathbf{f}}_{n-2}(p,t)}{\partial t} + 2\frac{\partial \hat{\mathbf{f}}_n(p,t)}{\partial t} + \frac{\partial \hat{\mathbf{f}}_{n+2}(p,t)}{\partial t}\\ &= (-rv\boldsymbol{\eta}_1 + i\frac{rv}{l}\boldsymbol{\eta}_3 - \frac{D(n-2)^2}{2})\hat{\mathbf{f}}_{n-2}(p,t)\\ &+ (-2rv\boldsymbol{\eta}_1 - Dn^2)\hat{\mathbf{f}}_n(p,t)\\ &+ (-rv\boldsymbol{\eta}_1 - i\frac{rv}{l}\boldsymbol{\eta}_3 - \frac{D(n+2)^2}{2})\hat{\mathbf{f}}_{n+2}(p,t)\end{aligned}, \quad (58)$$

which has the form

$$\mathbf{M}_1\frac{\partial \hat{\mathbf{f}}}{\partial t} = \mathbf{M}_2\hat{\mathbf{f}}, \quad (59)$$

where $\hat{\mathbf{f}}$ is a vector which consists of $\hat{\mathbf{f}}_n$'s. By truncating the $\mathbf{f}_n$ and $\boldsymbol{\eta}_i$ as (2L+1) by (2L+1) matrices and setting –N≤n≤N, one obtains two (2N+1)*(2L+1) by (2N+1)*(2L+1) tri-diagonal matrices

$$\mathbf{M}_1 = \begin{pmatrix} \cdots & & & & & & \\ & \mathbf{I} & 0 & 2\mathbf{I} & 0 & \mathbf{I} & \\ & & & & & & \cdots \end{pmatrix}, \quad (60)$$

$$\mathbf{M}_2 = \begin{pmatrix} \cdots & & & & & & \\ & \mathbf{m}_1 & 0 & \mathbf{m}_2 & 0 & \mathbf{m}_3 & \\ & & & & & & \cdots \end{pmatrix}, \quad (61)$$

where

$$\mathbf{m}_1 = -rv\boldsymbol{\eta}_1 + i\frac{rv}{l}\boldsymbol{\eta}_3 - \frac{D(n-2)^2}{2}\mathbf{I}, \quad (62)$$

$$\mathbf{m}_2 = -2rv\boldsymbol{\eta}_1 - Dn^2\mathbf{I}, \quad (63)$$

$$\mathbf{m}_3 = -rv\boldsymbol{\eta}_1 - i\frac{rv}{l}\boldsymbol{\eta}_3 - \frac{D(n+2)^2}{2}\mathbf{I}, \quad (64)$$

and $\mathbf{I}$ is the (2L+1) by (2L+1) identity matrix.

Because x=y=θ=ϕ=0 when t=0, the initial condition for equations (30) is defined as

$$f(g(x,y,\theta,\phi);t=0) = \delta(x)\delta(y)\delta(\theta)\delta(\phi). \quad (65)$$

As a result, $\hat{\mathbf{f}}(p,0)$ is an identity matrix, and the solution of equation (59) is

$$\hat{\mathbf{f}}(p,t) = e^{\mathbf{A}(p)t}, \quad (66)$$

where $\mathbf{A} = \mathbf{M}_1^{-1}\mathbf{M}_2$. (67)

Then, by inverse Fourier transform on SE(2), one obtains

$$f_n(g(x,y,\theta),t) = \int_0^{\infty} trace(\hat{\mathbf{f}}_n(p,t)\mathbf{U}(g,p))\,pdp \cdot \quad (68)$$

The desired time-evolving PDF is obtained by

$$f(g(x,y,\theta),\phi,t) = \sum_{n=-\infty}^{\infty} f_n(g(x,y,\theta),t)e^{in\phi} \cdot \quad (69)$$

To compute the reduced PDF $f(x,y,t)$, one integrates $f(g(x,y,\theta),\phi,t)$ as

$$f(x,y,t) = \int_{-\pi}^{\pi}\int_{-\pi}^{\pi} f(g(x,y,\theta),\phi,t)d\theta d\phi \cdot \quad (70)$$

By solving Fokker-Planck equation (30), one obtains PDFs like those in Fig.5.

V. CONCLUSION

In this paper, dead-reckoning error is studied in the context of different models of mobile robots with nonholonomic constraints where there is noise in the steering and/or drive systems. As one can see, the Fourier transform on SE(2) provides a powerful tool to solve the Fokker-Planck equations that describe the evolution of pose in these examples arising from the planar stochastic motion of those dynamic systems.

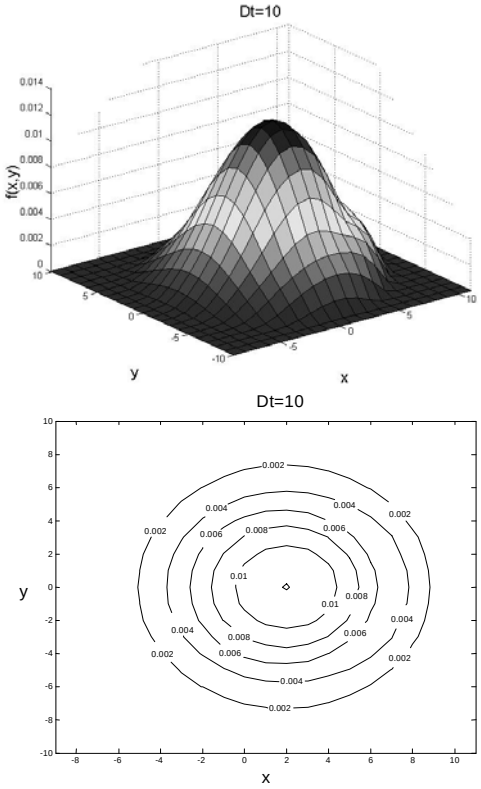

Fig.5 PDF of the position of the car model when Dt=10, r=v=1 and *l*=5 (L=5,N=6)

The results in this paper are obtained by assuming a constant spinning rate for the wheels, which guarantees such analytical intermediate results as (43) and (66). We are currently investigating cases in which the deterministic parts of wheel speeds and heading angles are variable. In the future, more attention will be given to the dead-reckoning errors caused by slipping and skidding of the wheels.

VI. ACKNOWLEDGEMENTS

We thank Mr. S. Ramakrishnan and Dr. Y. Wang for their input. This work was supported under NSF grant IIS-0098382.

VII. REFERENCES

[1] C. Tsai, "A localization system of a mobile robot by fusing dead-reckoning and ultrasonic measurements", *IEEE Trans. Instrumentation and Measurement*, vol.47, 1998, pp.1399-1404.

[2] H. Chung, L. Ojeda, J. Borenstein, "Accurate mobile robot dead-reckoning with a precision-calibrated fiber-optic gyroscope", *IEEE Trans. Robotics and Automation*, vol.17, 2001, pp.80-84.

[3] J. Horn, G. Schmidt, "Continuous localizatiion of a mobile robot based on 3D-laser-range-data, predicted sensor images, and dead-reckoning", *Robotics and Autonomous Systems*, vol.14, 1995, pp.99-118.

[4] M.V. Srinivasan, J.S. Chahl, S.W. Zhang, "robot navigation by visual dead-reckoning: inspiration for insects", *Int. J. Pattern Recognition and Artificial Intelligence*, vol.11, 1997, pp.35-47.

[5] J.H. Kim, H.S. Cho, "An improved dead reckoning scheme for a mobile robot using neutral networks", *Mechatronics*, vol.3, 1993, pp.625-425.

[6] J. Borenstein, "Internal correction of dead-reckoning errors with a dual-drive compliant linkage mobile robot", *J. Robotic Systems*, vol.12, 1995, pp257-273.

[7] M. Golfarelli, D. Mario, S. Rizzi, "Correction of dead-reckoning errors in map building for mobile robots", *IEEE Trans. Robotics and Automation*, vol.17, 2001, pp.37-47.

[8] G. Dudek, M. Jenkin, *Computational Principle of Mobile Robotics*, Cambridge University Press, 2000.

[9] D. Fox, W. Burgard, S. Thrun, A.B. Cremers, "Position estimation for mobile robots in dynamic environments", *Proc. 15th National Conf. on Artificial Intelligence (AAAI'98)*, 1998.

[10] N. Thrun, "Finding landmarks for mobile robot navigation", *Proc. IEEE Int. Conf. Robotics and Automation*, 1998, pp.958-963.

[11] D. Krantz, M. Gini, "Non-uniform dead-reckoning position estimate updates", *Proc. IEEE Int. Conf. Robotics and Automation*, 1996, pp.2061-2066.

[12] C.W. Gardiner, *Handbook of Stochastic Methods, 2nd Edition*. Springer, 1997.

[13] S. Ramakrishnan, *Stochastic Analysis of Nonholonomic Dynamical Systems*, MSE thesis, Johns Hopkins University, 2001.

[14] R.M. Murray, Z. Li, S.S. Sastry, *A Mathematical Introduction to Robotic Manipulation*, CRC Press, Boca Raton, 1994.

[15] G.S. Chirikjian, A.B. Kyatkin, *Engineering Applications of Noncommutative Harmonic Analysis*, CRC Press, Boca Raton, 2001.

[16] Y. Wang, *Applications of Diffusion Processes in Robotics, Optical Communicatins and Polymer Science*, PhD dissertation, Johns Hopkins University, 2001.

[17] Y. Wang, G.S. Chirikjian, "A diffusion-based algorithm for workspace generation of highly articulated manipulators", *Proc. IEEE Int. Conf. Robotics and Automation*, 2002, pp.1525-1530.